Acta Astronautica 228 (2025) 1056–1065

Contents lists available at ScienceDirect

Acta Astronautica

journal homepage: www.elsevier.com/locate/actaastro

Experimental test and numerical validation for evaluating the dynamics of the In-Line Damper for the E.T.PACK-F project

Giulio Polato [a,b,*], Matteo Urbinati [b], Andrea Valmorbida [b,c], Giovanni Anese [c], Alice Brunello [b], Samantha Salmistraro [b], Sebastiano Chiodini [b,c], Giacomo Colombatti [b,c], Enrico C. Lorenzini [b,c]

[a] Department of Physics, University of Trento, Via Sommarive 14, Povo (TN), 38123, Italy
[b] Department of Industrial Engineering (DII), University of Padova, via Venezia 1, Padova (PD), 35131, Italy
[c] CISAS "G.Colombo", University of Padova, Via Venezia 15, Padova (PD), 35131, Italy

ARTICLE INFO

Keywords:
Electrodynamic tether
In-Line Damper
Space debris deorbiting
Experimental testing
Numerical modeling

ABSTRACT

The E.T.PACK-F project, funded by the European Innovation Council (EIC), seeks to investigate and to advance electrodynamic tether technologies (EDT) by developing two flight modules connected through an aluminum tether to demonstrate space debris deorbiting. In this context the In Line Damper (ILD) plays an important role for the stability of the entire system during the deployment of the tether and the deorbiting phase. In this paper we want to present a study on the ILD behavior when subjected to an external load, due to the initial separation of the two modules. In particular, we tested the device at the SPARTANS facility of the University of Padova, utilizing a low-friction glass table which can accommodate the experimental setup. The collected data were correlated and studied numerically using an optimization process, which enables to tune the parameters needed for describing the ILD motion, using a 2D model. In conclusion, the results successfully demonstrate modeling of the ILD dynamics, enabling the extraction of characteristic parameters, revealing non-linear tendencies and providing more insights into the mechanical response of the device.

1. Introduction

In the last few decades, the escalating challenge of man-made space debris has raised serious concerns about the success of future space missions and the space community has turned its attention to innovative "green" deorbiting technologies. Electrodynamic Tethers (EDT) stand out in this endeavor due to their passive and propellantless nature, offering significant potential in addressing space debris challenges, particularly in low Earth orbit (LEO).

The E.T.PACK-F project [1], funded by the European Innovation Council (EIC), aims to develop a TRL 8 product prototype, known as Deorbit Kit, leveraging EDT technology to safely deorbit end-of-life satellites. The device comprises two modules: the first one accommodates the deployment mechanism (DMM) and the second one hosts the hollow cathode electron emitter (EMM). Once in orbit, a 470-meter-long aluminum tape will be deployed, and the electron emitter will initiate current flow in the tether, generating a Lorentz drag force through interaction with the geomagnetic field, effectively aiding in the deorbiting of the satellite.

During satellite deorbiting, the Lorentz force induces tether oscillations (libration) that may escalate without energy damping, potentially leading to system instability before reentry into the upper atmosphere. As part of the E.T.PACK-F consortium, the University of Padova has developed the In-Line Damper (ILD), a passive mechanical device designed to dissipate energy through tension variations in the tether [2]. Moreover and equally important, the ILD impacts the dynamics of the modules during the initial phase of their separation. To ensure successful separation, a thorough understanding of the ILD's influence on relative dynamics and the implementation of a suitable sequence of operations are essential.

Our research group has developed both software tools and laboratory setups to simulate and experimentally verify the initial phase of the E.T.PACK-F module separation.

We have developed a MATLAB program to simulate the complete dynamics of the EEM module during the early separation phase. Specifically, the module is modeled as rigid bodies with complete 3 degrees

* Corresponding author.
E-mail addresses: giulio.polato@unitn.it (G. Polato), matteo.urbinati@studenti.unipd.it (M. Urbinati), andrea.valmorbida@unipd.it (A. Valmorbida), giovanni.anese@phd.unipd.it (G. Anese), alice.brunello@unipd.it (A. Brunello), samantha.salmistraro@unipd.it (S. Salmistraro), sebastiano.chiodini@unipd.it (S. Chiodini), giacomo.colombatti@unipd.it (G. Colombatti), enrico.lorenzini@unipd.it (E.C. Lorenzini).

https://doi.org/10.1016/j.actaastro.2024.12.029
Received 24 July 2024; Received in revised form 9 November 2024; Accepted 15 December 2024
Available online 2 January 2025

of freedom dynamics and the tether as a sequence of lumped masses properly connected, accounting for the elastic and damping effects of the ILD.

The laboratory setup utilizes the unique SPARTANS facility [3], consisting of two platforms capable of low-friction movement on a 3 m × 2 m testing table via an air-cushion system, that can reproduce the separation dynamics between the two modules.

This paper presents numerical results obtained by tuning the experimental data with the MATLAB simulator and experimental results obtained with the SPARTANS facility. The objective is to provide deeper insights into ILD behavior during the early phase of the modules separation, focusing on characterizing the mechanical response of the ILD while the motion of the modules is confined to a 2D dynamics only.

2. The In-Line Damper (ILD)

Generally speaking, the ILD is a compact box housing a spring linked to the EEM through a cable. This spring is forced to move along a particular path, that has an influence on the damping coefficient. Consequently, the ILD functions as a mass–spring–damper system, illustrated in Fig. 1.

The purpose of this device is to decrease the stiffness of the aluminum tether by fine-tuning the spring coefficient and to dissipate energy through adjustment of the damping coefficient.

Moreover, these coefficients are of critical importance during the deployment phase. Ref. [4] shows that the stiffness and damping coefficients directly impact the amount of propellant needed to control the attitude of the DMM module.

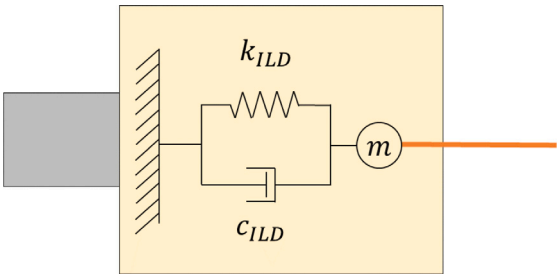

Fig. 1. ILD mass–spring–damper model.

2.1. ILD design

The current design of the In-Line Damper represents an advancement over the initial prototype (see [5]), which was tested to evaluate its impact on tether dynamics.

The design requirements for the new version are similar to those of the prototype and can be summarized as follows:

- REQ 1. Electrical continuity: the ILD shall maintain the electrical continuity between the tether and the spacecraft.
- REQ 2. Mechanical continuity: The ILD is required to maintain the desired connection with regards to stiffness, damping, and deformation. Specifically, the ILD stiffness should be significantly lower than the tether stiffness, particularly at shorter tether lengths.
- REQ 3. Miniaturization: the ILD shall be able to fit on board of a 12U CubeSat with a parallelepiped shape. The maximum volume is 100 cm^3.
- REQ 4. Tape tether: the ILD shall accommodate a tape tether with a maximum thickness of 50 μm and a maximum width of 25 mm.

The primary reason for updating the design lies in the fact that the ILD is subjected to external forces during separation that are greater than the tether forces during deployment and later during the deorbiting phase.

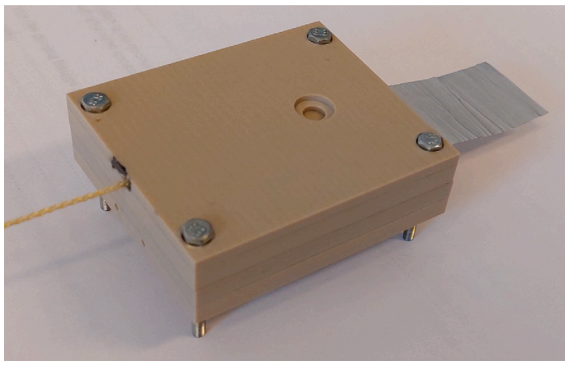

Fig. 2. ILD PEEK prototype.

Consequently, since the stiffness should be much lower than the tether stiffness (REQ 2), in order to absorb the amount of energy acting on the tether during the separation, the ILD must have a sufficiently long stroke, which was not considered in the previous design.

Moreover, the requirements on the dimensions (REQ 3) are increased and it is possible to improve the internal design.

2.2. ILD testing prototype

For the laboratory test described in this paper, it was used an ILD made out of PEEK. This material is widely used in space applications, particularly for its thermo-mechanical properties, which makes it one of the most reliable polymers for the space environment. It is also possible to manufacture it with 3D printing method that makes it suitable for prototyping.

Fig. 2 shows a picture of the ILD prototype made out of PEEK and it is possible to understand where the aluminum tape is attached at one end and on the other side the exiting cable attached to the internal spring.

The stiffness and damping coefficient were determined by using an optimization process, as described in the following sections.

3. Mathematical model

A schematic representation of the entire system during the early separation phase is shown in Fig. 3.

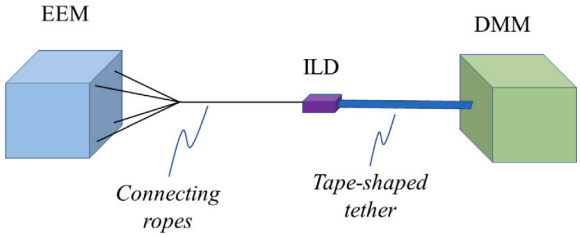

Fig. 3. System representation.

The EEM is connected through four attaching points, while the DMM has only one attaching point. The ILD is close and connected to the EEM by a Kevlar cable and to the DMM by the aluminum tape.

For the simulations only the EEM motion is considered, and the DMM is assumed to be fixed. In general, the equations that describe the motion of a 3D rigid body are the following:

$$\mathbf{F} = m \cdot \ddot{\mathbf{x}} \tag{1}$$

$$\mathbf{T} = \boldsymbol{I} \cdot \dot{\boldsymbol{\omega}} \tag{2}$$

Hence, for the integration of the above equations, referring to Fig. 4, the equations become:

$$\dot{\mathbf{x}}_E = \mathbf{v}_E \tag{3}$$

$$\ddot{\mathbf{x}}_E = \frac{\sum \mathbf{F}_{i,E}}{m_E} \tag{4}$$

where $F_{i,E}$ are the thrust and wire tension forces.

$$\dot{\mathbf{q}} = \frac{1}{2}\boldsymbol{Q}(q) \cdot \boldsymbol{\omega}_E \tag{5}$$

$$\dot{\boldsymbol{\omega}}_E = \boldsymbol{I}_E^{-1}\left(\sum \boldsymbol{\tau}_{i,E} - \boldsymbol{\omega}_E \times (\boldsymbol{I}_E \cdot \boldsymbol{\omega}_E)\right) \tag{6}$$

where $\boldsymbol{\tau}_{\mathbf{i,E}}$ are the torques due to the thrust and tension forces, $\boldsymbol{I}_E$ is the inertia of the EEM, and m_E is the mass of the module.

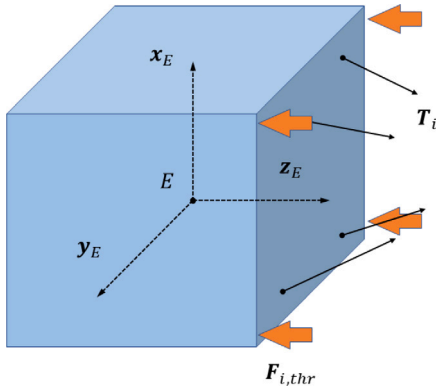

Fig. 4. EMM representation.

For what concerns the cable, it is used the lumped mass model. Referring to Fig. 5 the equations that describe the dynamics are the following:

$$\dot{\mathbf{x}}_i = \mathbf{v}_i \tag{7}$$

$$\ddot{\mathbf{x}}_i = \frac{\sum \mathbf{F}_{i,j}}{m_i} \tag{8}$$

$$\mathbf{F}_{i,j}(\Delta l_{i,j}) = \begin{cases} 0, & \Delta l_{i,j} < 0 \\ (k_{ILD}\Delta l_{i,j} + c_{ILD}\Delta \dot{l}_{i,j})\,\hat{\mathbf{u}}_{i,j}, & \Delta l_{i,j} \geq 0 \end{cases} \tag{9}$$

where $\Delta l_{i,j} = \|\mathbf{x}_i - \mathbf{x}_j\| - l_{0\,i,j}$, $\Delta \dot{l}_{i,j} = (\mathbf{x}_i - \mathbf{x}_j) \cdot \hat{\mathbf{u}}_{i,j}$ and finally $\hat{\mathbf{u}}_{i,j} = ((\mathbf{x}_i - \mathbf{x}_j)) \,/\, \|\mathbf{x}_i - \mathbf{x}_j\|$.

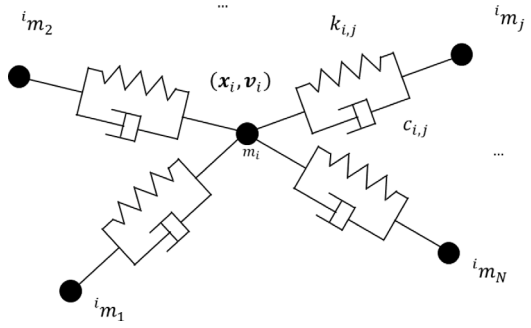

Fig. 5. Lumped mass model.

For what concern the ILD, the mathematical model is the same as a mass lumped model, but since the elastic contribution of the force depends from the motion direction, the stiffness coefficient is:

$$k_{ILD}(\Delta \dot{l}_{i,j}) = \begin{cases} 0, & \Delta \dot{l}_{i,j} < 0 \\ const, & \Delta \dot{l}_{i,j} \geq 0 \end{cases} \tag{10}$$

This behavior is due to the fact that in the heavier experimental setup the ILD is not fully able to recover its elastic stretch. Only when the cable is almost unloaded is the ILD able to fully recover the stretch. The experimental results highlight this behavior.

In order to describe the experimental observations, the mathematical models include some assumptions listed below:

- The module that represents the EEM can move only along two directions (x and y) and can rotate only along the vertical axis (z), so the equations are reduced for a 2D case, as mentioned earlier.
- The gravitational effects on the cable are not taken into account because their contribution is negligible compared to the tension in the cable during the elongation of the ILD.

4. Experimental set up

To validate experimentally the separation dynamics between the two modules of the E.T.PACK-F system, the SPARTANS testing facility [6] was utilized. This setup includes a 3 m x 2 m testing table over which two modules, called Translational Modules (TMs), can smoothly move with low friction, due to a system of air cushion that enables them to float. The modules have 3 degrees of freedom each: translation in the x and y directions on the table, and rotation around the vertical (z) axis. A set of six external infra-red (IR) cameras, mounted on the ceil of the laboratory, is employed to accurately measure both position and orientation of each module.

Specifically, a computer grabs the images recorded by the six IR cameras and elaborates them to detect and track specific IR retro-reflective markers attached to the modules in known positions [7]. These markers are arranged in unique patterns for each module, allowing for specific identification and spatial tracking. The detected positions of these markers are then transmitted via Wi-Fi to another computer, where a program written in MATLAB recognizes each module's marker pattern and logs its position and orientation.

To reproduce in laboratory the relative dynamics between the DMM and the EEM during their separation, the smallest SPARTANS module was modified and employed to represent the EEM, with the DMM mimicked by a static structure made of aluminum beam profiles and attached to the perimetral frame of the testing table. Specifically, the TM representing the EEM (Fig. 6) consists of two main parts: a lower translation platform equipped with a fluid system to supply three air-bearings and an upper control platform.

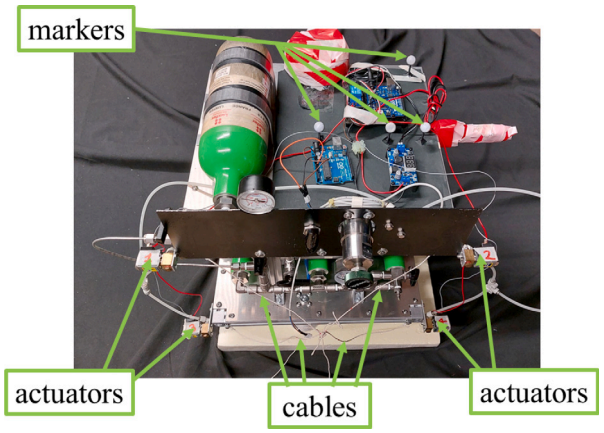

Fig. 6. SPARTANS small Translational Module (TM) modified for testing the E.T.PACK-F separation dynamics.

The latter hosts a cold-gas propulsion system with four actuators to perform the separation phase. The upper control platform also hosts four IR markers specifically positioned to simplify the reconstruction of the module's trajectory, such as a marker located at the predicted center of mass position. Furthermore, the position of both the actuators and the attaching points of the inert cable to the TM are identified to be representative of the tethered system.

The control of the thrust is carried out by an Arduino Uno Wi-Fi able to switch on and off the corresponding four solenoid valves.

The Arduino board is operated remotely via a dedicated web interface, allowing users to issue commands that open the valves for set durations, after which they close automatically.

Two types of preparatory tests were conducted to characterize the SPARTANS TM [8]. The first set of tests aimed to estimate the TM mass, its center of mass position in the x-y plane and its moment of inertia around the vertical z-axis. These properties are crucial for understanding the dynamics of the TM on the testing table, and an accurate estimation of these is important. The second set of tests was performed to estimate the force exerted by the four actuators onboard the TM module. Subsequently, experimental tests were carried out to examine the behavior of the ILD during the early phase of the module's separation.

4.1. Preparatory test

For the characterization of the inertia module, a torsional pendulum was used, where the stiffness of an aluminum stem and the oscillation period of the support frame were measured before the test.

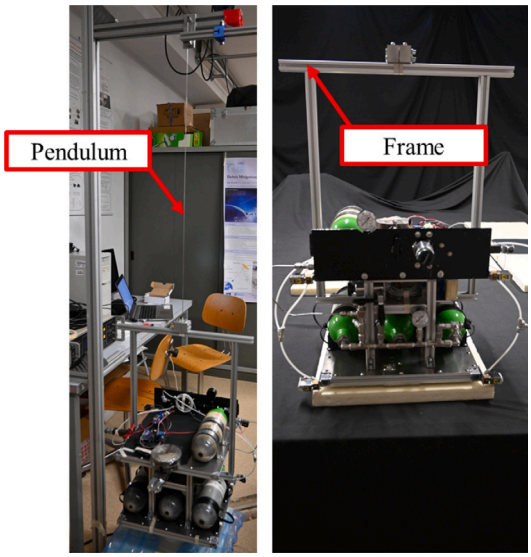

Fig. 7. Setup for calculating the inertia of the system.

The TM was attached on a supporting frame and, using a laser fixed to the structure to which the pendulum was connected, it was possible to retrieve the inertia by calculating the oscillation period. The experimental setup described is shown in Fig. 7.

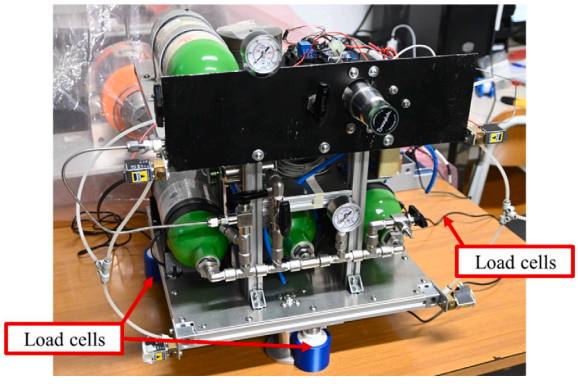

Fig. 8. Experimental setup used to measure the mass of the floating module and the position of its center of mass on the x-y plane, with the three calibrated load cells (the three cylindrical elements at the platform base; one of them is not visible in the figure).

In Fig. 8 it is shown the experimental set up used to estimate the position of the center of mass; it embeds three load cells located at known positions with respect to the body frame of the module. The forces measured with the load cells are elaborated using a MATLAB script to estimates the position the barycenter and the mass of the module. To accurately estimate these two parameters the cells were previously calibrated [9].

This activity was necessary to understand the extent of the TM imbalance, allowing the balancing of the system by aligning the center of gravity with the geometric center. For this purpose, additional counterweights were used.

Finally, the parameters of the module measured during these tests and needed in the mathematical model used in the simulations are reported in Table 1, where the "mp" index is referred to the "middle point", that is the point where the four cables are linked together. The coordinates of the system are given in Fig. 4.

Table 1
Parameters of the spring and wire.

Parameters	Value
m_E	15.90 ± 0.025 [kg]
I_E	0.412 ± 0.027 [kg m^2]
l_{T1-mp}	223 ± 0.25 [mm]
l_{T2-mp}	223 ± 0.25 [mm]
l_{T3-mp}	220 ± 0.25 [mm]
l_{T4-mp}	221 ± 0.25 [mm]
l_{mp-ILD}	235 ± 0.25 [mm]
r_{T1}	[111.0 155.0 167.5] ± 0.5 [mm]
r_{T2}	[−111.0 153.0 167.5] ± 0.5 [mm]
r_{T3}	[111.0 153.5 167.5] ± 0.5 [mm]
r_{T4}	[−111.0 153.5 167.5] ± 0.5 [mm]
r_{F1}	[140.7 184.8 201.1] ± 0.5 [mm]
r_{F2}	[−141.6 184.5 198.6] ± 0.5 [mm]
r_{F3}	[138.7 −184.5 199.7] ± 0.5 [mm]
r_{F4}	[−141.3 −184.0 198.3] ± 0.5 [mm]

4.2. Thrust test setup

To measure the force actuated by the four actuators on board the TM, the experimental setup shown in Fig. 9 was employed.

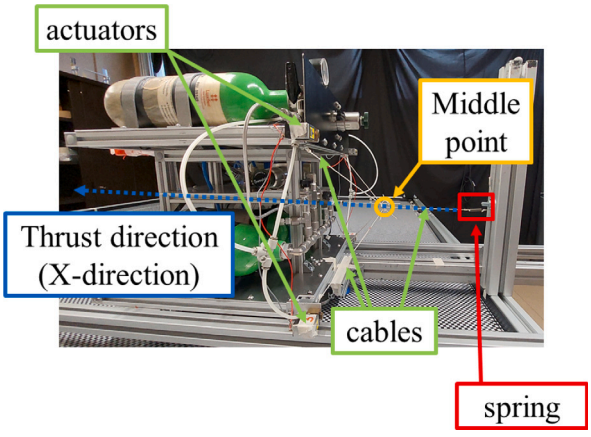

Fig. 9. Thrust test setup.

One tip of a spring with known elastic constant is attached to the external fixed frame of the testing table through an aluminum profile, while the other tip of the spring is attached to the cable coming from the floating module.

By activating the actuators for 40 s, it was possible to characterize the total thrust exerted along the spring axis and the elastic and damping coefficients of the wire, as shown in Section 5.1. The TM was set in an initial position such that the spring and wire system has a small pretension. In that way, it was possible to ensure that the motion of the TM is a direct consequence of the spring elongation.

4.3. ILD test setup

The ILD was anchored to a fixed structure, attached to the edge of the testing table. The thrust force was impressed using four solenoid valves with nozzles positioned at the corners of the module facing the

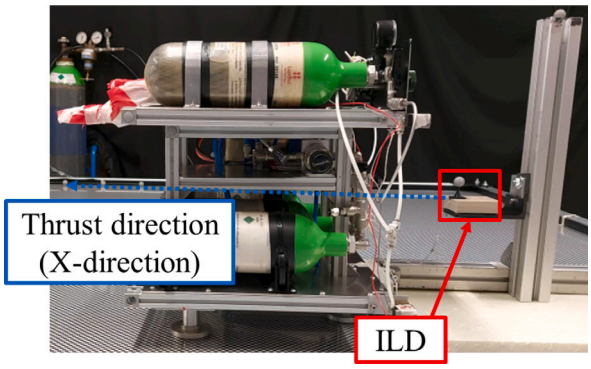

Fig. 10. ILD test setup.

ILD, as shown in Fig. 10.

The distance between the module and the ILD was fixed, by using an infrastructure which allows to have the same initial condition on the position and orientation.

Moreover, this distance was chosen such that the cables are in a slack condition and during the thrust phase, which lasts 10 s for each test, the module was pushed away from the ILD. During the test, the cables get tensioned, the ILD reaches an equilibrium point and the module stops at a fixed distance from the ILD. The test ended when the solenoid valves of the thrusters close.

5. Optimization process

To analyze the experimental data obtained during the tests, an optimization process is needed for estimating the missing physical parameter. Moreover, a simplified 2D mathematical model is used to describe the dynamics of the floating module during the actuators characterization and the ILD characterization test campaigns.

The optimization process progressed in the steps described below:

1. Concerning the thrust characterization tests, it is possible to estimate the thrust variation over time, the stiffness and the damping coefficient of the entire system.
2. Using only the initial part of the ILD tests, when the system is not subjected to the cable tension, key parameters such as the starting time of the test t_0, the initial thrust, the thrust unbalance α (see below) and the initial condition y_0, can be estimated. Parameters x_0 and θ_0 were assessed as the averages of their respective values over a brief time interval immediately preceding t_0.
3. The last step is the tuning of the ILD stiffness and damping coefficient using the entire experimental data acquired during the ILD characterization test campaign.

5.1. Thrust test optimization

The model used to describe the thrust tests is the monodimensional response of a mass–spring–damper system to a ramp input $F(t) = F_0 + F_1 t$, where $x_0 = 0$.

$$x(t)_{ramp} = x_0 + \frac{F_0}{k}\left[1 - e^{-\zeta\omega_n t}\left(\cos\omega_s t + \frac{\zeta}{\sqrt{1-\zeta^2}}\sin\omega_s t\right)\right] + \frac{F_1}{k}\left\{t - \frac{2\zeta}{\omega_n}\left[1 - e^{-\zeta\omega_n t}\left(\cos\omega_s t - \frac{\zeta^2}{\sqrt{1-\zeta^2}}\sin\omega_s t\right)\right]\right\} \tag{11}$$

where $\omega_s = \sqrt{1-\zeta^2}\,\omega_n$ is the damped natural frequency of the system, ω_n is the natural frequency of the system, x_0 is the initial position, F_0 is the initial thrust force, F_1 is the slope of the ramp, k is the stiffness of the system and ζ is the damping ratio. For the optimization, a non-linear regression was used, since in this case the solution is exact, hence there is no need to integrate the equation of the motion. The cost function is the sum of the square of the residuals (SSR).

$$x(t) = \begin{cases} x_0, & t < t_0 \\ x(t)_{ramp}, & t \geq t_0 \end{cases} \tag{12}$$

In order to study the problem from a mono-dimensional point of view, the experimental data representing the $x(t)$ in Eq. (12) is the distance between the origin of the inertial system and the point where the four cable are attached each other (middle point). The position of the system is supposed constant at an initial value x_0 when $t < t_0$, and after the activation of the thruster at $t = t_0$ it follows the motion law presented in Eq. (11). The position of the middle point is assumed to be fixed relative to the TM, since all four cables remain in tension throughout the duration of the tests. Using this assumption, it is possible to calculate the position of the middle point, using the position and the orientation of the module.

The stiffness and the damping coefficient of the cable are calculated using the following equations:

$$\frac{1}{k_{cable\_tot}} = \frac{1}{k_{sys}} - \frac{1}{k_{spring}} \tag{13}$$

$$\frac{1}{c_{cable\_tot}} = \frac{1}{c_{sys}} - \frac{1}{c_{spring}} \tag{14}$$

where k_{sys} and c_{sys} are the stiffness and damping coefficient of the system respectively, k_{spring} and c_{spring} are the stiffness and damping coefficient of the spring respectively.

It is important to notice from the equations presented above that the stiffness of the system is expected to be closer to the value of the spring stiffness. That is because the spring dominates the elastic response, given that the cables are stiffer. Similarly, the damping coefficient is also assumed to be primarily influenced by the spring.

5.2. Initial condition optimization

Referring to Fig. 11, for the optimization of the initial conditions of the ILD test it is considered a 2D mathematical model describing the dynamic of the module which is free to move over the testing table and is subjected to two external forces that are not equal. This inequality accounts for two contributions: the forces actuated by each actuators are slightly different; the values of the friction forces between the air-bearings and the testing table are slightly different as well. As a consequence, the two thrust forces are not symmetric with respect to the X direction. Moreover, in the mathematical model it was assumed that the module starts in a static condition, hence $\dot{\mathbf{r}}_{Mi} = \ddot{\mathbf{r}}_{Mi} = \dot{\theta}_{Mi} = \ddot{\theta}_{Mi} = 0$.

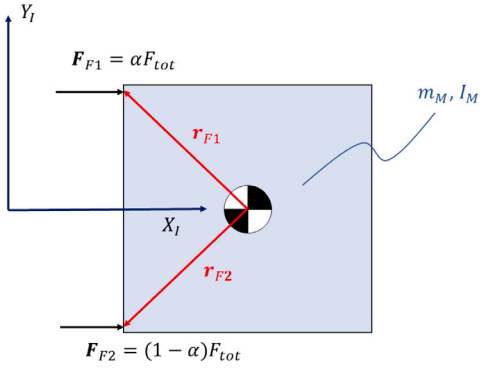

Fig. 11. 2D free moving model.

Referring to Fig. 11, m_M and I_M are the mass and the inertia of the module, respectively, F_{tot} is the total thrust force, α the thrust unbalance factor, r_{F1} and r_{F2} are the position of the actuators with respect to the body frame, r_M and θ_M are the position of the floating module barycenter and its orientation.

During this process, the optimized variables are the starting time of the "thrust phase" t_0, the total thrust force F_{tot}, the thrust unbalance factor α and the y coordinate initial position y_0.

Finally, the cost function is a weighted sum of the SSR of the distance of the module, while the second SSR focuses the residuals related to the orientation of the module. The reason for having a weighted sum is due to the fact that the orientation of the module is subject to larger estimation errors compared to position errors. Consequently, a higher "optimization priority" is assigned to the position than to the orientation.

5.3. ILD tests optimization

The final part consists in the optimization of the ILD parameters. The mathematical model used to represent the dynamics of the system in these tests is shown in Fig. 12. A simplified 2D model is considered, similarly to the previous tests.

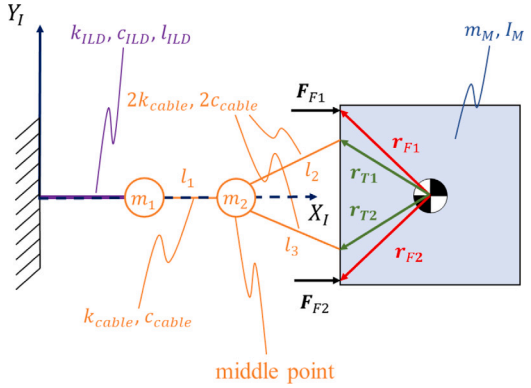

Fig. 12. 2D ILD tests model.

Referring to Fig. 12, in addition to the symbols used in Fig. 11, r_{T1} and r_{T2} are the position of the attaching point of the cable to the module with respect to the body frame, l_{ILD} is the length of the ILD that is not considered equals to zero, because if so it is induced some higher frequencies on the system which is not a realistic behavior, k_{ILD} and c_{ILD} are the stiffness and damping coefficients of the ILD, l_1, l_2 and l_3 are the three length of the cable that are almost identical and for this reason k_{cable} and c_{cable}, that are the stiffness and damping coefficients of the cable, are assumed to have the same value for all the cables, m_1 and m_2 are the lumped mass of the cables, where they represent the attaching point of the ILD to the cable and the middle point respectively.

The reason why the factor of two is applied to the cable attached to the module is because there are actually four cables, not just two. As a result, to accurately account for their stiffness and damping coefficients, the original values need to be doubled.

An initial estimate of the cable stiffness and damping can be derived from the values obtained in the first optimization using the following equations:

$$\frac{1}{k_{cable\_tot}} = \frac{1}{k_{cable}} + \frac{1}{2k_{cable} + 2k_{cable}} \tag{15}$$

$$\frac{1}{c_{cable\_tot}} = \frac{1}{c_{cable}} + \frac{1}{2c_{cable} + 2c_{cable}} \tag{16}$$

That becomes:

$$k_{cable} = \frac{5}{4} k_{cable\_tot} \tag{17}$$

$$c_{cable} = \frac{5}{4} c_{cable\_tot} \tag{18}$$

For this process, the optimized variables are the stiffness of the ILD k_{ILD}, the damping coefficient of the ILD c_{ILD} and the initial orientation of the module θ_{Mi}.

Finally, the cost function takes into account the weighted sum of three different SSRs: the distance of the midpoint where the cables connect, the distance of the barycenter, and the orientation of the module.

The reason for considering the first SSR is that, during the optimization process, it was observed that the estimated value of the cable stiffness and the damping coefficient were too low to explain the high frequency response observed by calculating the center distance.

In addition, the SSR of the orientation of the module was also compared with the relative orientation to the initial estimated orientation. The reason is that also the initial absolute orientation could be affected by a bias that is difficult to control during the test.

During the optimization process, it was noticed that the stiffness and damping coefficients always tend to diverge towards the upper bound of the optimization, and this causes the other parameters to diverge towards their upper bound as well. In order to avoid this problem, the stiffness and damping coefficient of the cable were assumed to be fixed at a certain value that is high enough to describe the behavior of the cable.

Nevertheless, the chosen value was used to compare it with the theoretical stiffness of the spring and to check if the value found falls within the tolerances.

6. Results and discussion

In this section, the results are organized into four parts: one focuses on the experimental results, and the other three are dedicated to each respective optimization process. Specifically, in this paper are reported six test results obtained from the experimental campaign, labeled from T1 to T6. In addition, the results are presented with an associated uncertainty at a 95% confidence level.

6.1. Experimental results

Referring to Figs. 13 and 14, the results obtained are shown synchronized at time $t_0 = 0$, for a better comparison.

The results show that the module exhibits similar behavior in terms of the distance of the barycenter from the origin of the inertial system during the first ten seconds, which is the "thrust phase". However, it tends to diverge afterward (Fig. 13).

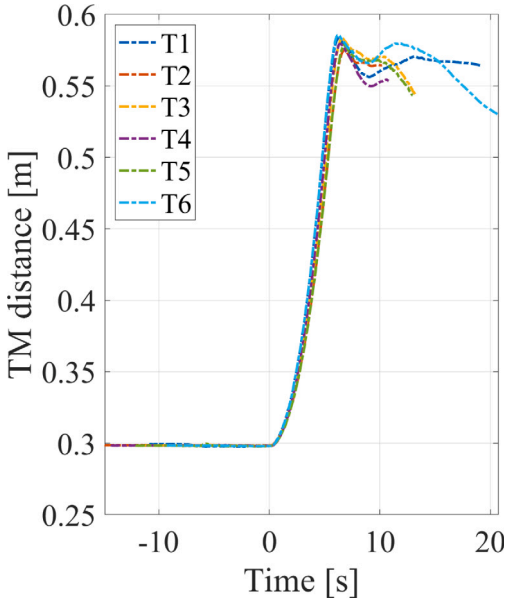

Fig. 13. Experimental results, barycenter distance of the TM. (For interpretation of the references to color in this figure legend, the reader is referred to the web version of this article.)

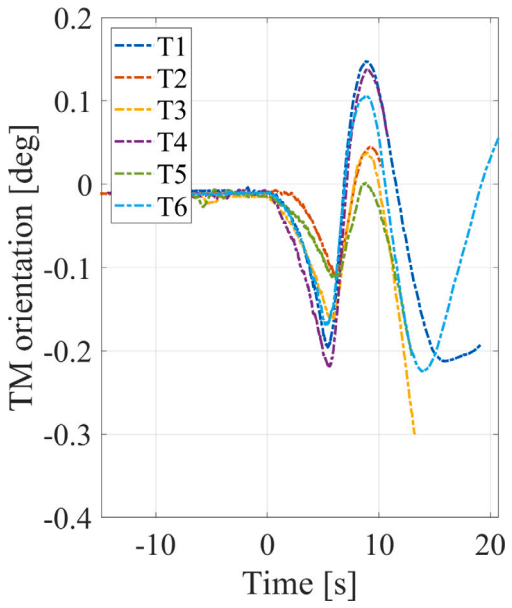

Fig. 14. Experimental results, absolute orientation of the TM. (For interpretation of the references to color in this figure legend, the reader is referred to the web version of this article.)

Additionally, there is a noticeable difference in the slopes of the curves during the "thrust phase" attributed to the varying thrust during each test. Further explanation of the causes is provided in the section below.

On the other hand, the orientation appears to vary for each test. This discrepancy arises because it is challenging to obtain an absolute estimation of the relative orientation between the ILD and the module, as depicted in Fig. 14.

6.2. Thrust test optimization results

In Fig. 15 are compared the position of the midpoint obtained from the experimental data and the nonlinear regression obtained with the model previously described. Moreover, in Table 2 are reported the parameters obtained from the regression.

Table 2
Parameters of the thrust test.

Parameters	Value
k_{sys}	4.302 ± 0.002 [N/m]
c_{sys}	0.327 ± 0.003 [Ns/m]
F_1	$(7.09 \pm 0.09) \times 10^{-4}$ [N/s]
$mean(Res)$	0.09×10^{-3}
$max(Res)$	1.54×10^{-3}
SSR	0.75×10^{-3}

The F_1 parameter is positive because two effects are acting on the module during the test. The first effect is the mass of the module, which is slowly decreasing. However, in this model the mass is considered to be constant and this translates into an increasing thrust force. Secondly, the supply pressure effect (SPE) increases the pressure at the outlet of the pressure regulator, while the inlet pressure decreases.

In the following Table 3 are reported the values of the spring and cable stiffness, while the values of the damping coefficient are only an estimate, assuming the spring with the lower value of the damping coefficient. The associated uncertainty for the spring parameters is assumed to be 15% of the nominal value, due to the absence of available data. It is important to note that the associated uncertainties for the cable stiffness and the damping coefficient are slightly high, which was the primary reason for not utilizing these values for the final optimization.

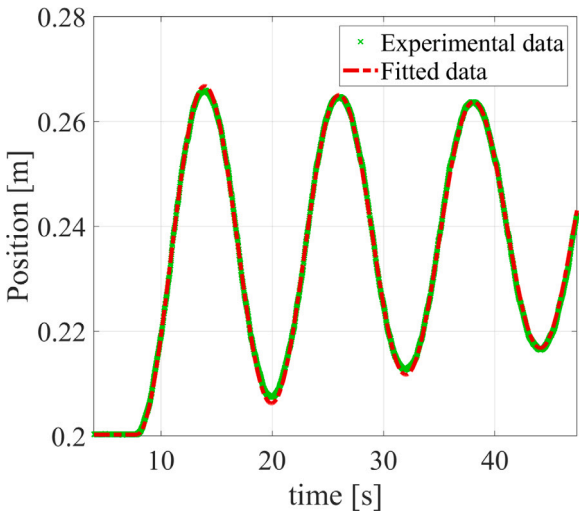

Fig. 15. Comparison between the experimental data and the non-linear regression obtained. (For interpretation of the references to color in this figure legend, the reader is referred to the web version of this article.)

Table 3
Parameters of the spring and wire.

Parameters	Value
k_{spring}	4.641 ± 0.68 [N/m]
c_{spring}	0.360 ± 0.054 [Ns/m]
k_{cable_tot}	58.91 ± 109.51 [N/m]
c_{cable_tot}	3.452 ± 5.31 [Ns/m]

6.3. Initial condition optimization results

The results for these tests are reported in Table 4, where the main parameters optimized for each test are shown.

Table 4
Parameters of the initial condition optimization.

Parameters	T1	T2
t_0 [s]	10.82 ± 0.01	14.89 ± 0.02
F_{tot} [N]	0.277 ± 0.001	0.223 ± 0.002
α	0.551 ± 0.001	0.526 ± 0.001
y_0 [m]	-0.01 ± 0.003	0.009 ± 0.009
$mean(Res)$	0.05×10^{-3}	0.311×10^{-3}
$max(Res)$	2.65×10^{-3}	4.639×10^{-3}
SSR	0.5×10^{-3}	20.6×10^{-3}
Parameters	T3	T4
t_0 [s]	11.76 ± 0.02	14.30 ± 0.03
F_{tot} [N]	0.242 ± 0.002	0.251 ± 0.004
α	0.553 ± 0.001	0.581 ± 0.002
y_0 [m]	-0.001 ± 0.051	-0.001 ± 0.159
$mean(Res)$	0.805×10^{-3}	1.652×10^{-3}
$max(Res)$	5.347×10^{-3}	9.374×10^{-3}
SSR	163.5×10^{-3}	634.3×10^{-3}
Parameters	T5	T6
t_0 [s]	12.06 ± 0.02	9.27 ± 0.01
F_{tot} [N]	0.222 ± 0.002	0.279 ± 0.001
α	0.532 ± 0.001	0.549 ± 0.001
y_0 [m]	0.009 ± 0.007	-0.009 ± 0.003
$mean(Res)$	0.385×10^{-3}	0.229×10^{-3}
$max(Res)$	3.916×10^{-3}	2.813×10^{-3}
SSR	34.4×10^{-3}	13.2×10^{-3}

In Table 4 it can be seen that the estimated unbalance coefficient $\alpha > 0.5$, meaning that the initial angular velocity is clockwise, as shown in Fig. 14.

Moreover, looking at the mean value of the residuals, the first and last tests are the ones that fit the model better, due to the fact that the initial angular velocity was really close to zero.

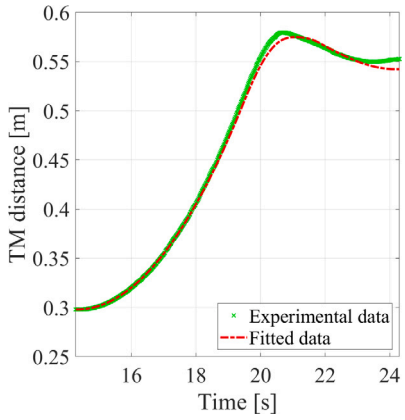

Fig. 16. T4, comparison between the barycenter distance of experimental and simulated data. (For interpretation of the references to color in this figure legend, the reader is referred to the web version of this article.)

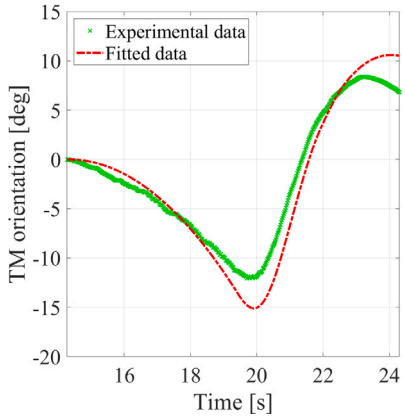

Fig. 17. T4, comparison between the orientation of experimental and simulated data. (For interpretation of the references to color in this figure legend, the reader is referred to the web version of this article.)

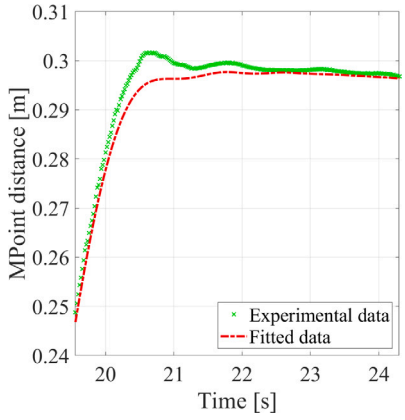

Fig. 18. T4, comparison between the middle point distance of experimental and simulated data. (For interpretation of the references to color in this figure legend, the reader is referred to the web version of this article.)

6.4. ILD tests optimization results

As previously described, the values of the stiffness and the damping coefficients are summarized in Table 5, where it is also given the estimated value of the spring coefficients that falls into the theoretical value tolerances previously found (see Table 3).

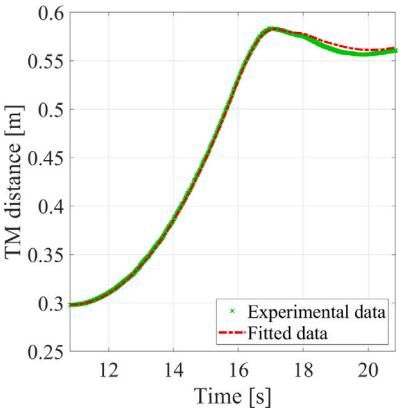

Fig. 19. T1, comparison between the barycenter distance of experimental and simulated data. (For interpretation of the references to color in this figure legend, the reader is referred to the web version of this article.)

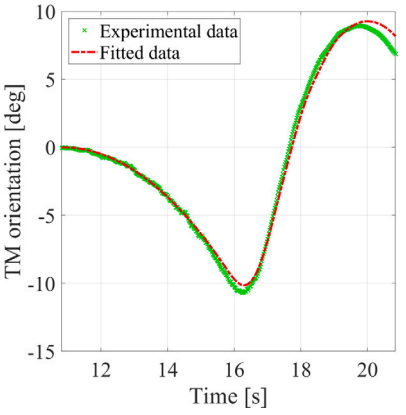

Fig. 20. T1, comparison between the orientation of experimental and simulated data. (For interpretation of the references to color in this figure legend, the reader is referred to the web version of this article.)

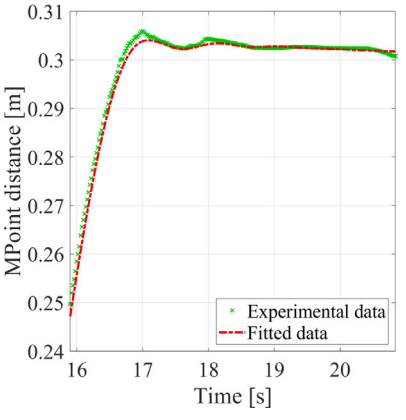

Fig. 21. T1, comparison between the middle point distance of experimental and simulated data. (For interpretation of the references to color in this figure legend, the reader is referred to the web version of this article.)

For what concerns the ILD tests, the results are summarized in the following Table 6.

In addition, only the results of the test with the highest and lowest mean of the residuals values are reported in this paper (i.e., T1 and T4). The results of other tests that fall in the middle range are generally similar and are not shown for brevity.

Table 5
Parameters of the wire coefficients.

Parameters	Value
k_{cable}	930 [N/m]
c_{cable}	2 [Ns/m]
k_{spring}	4.322 [N/m]
c_{spring}	0.391 [Ns/m]

Table 6
Parameters of the ILD test optimization.

Parameters	T1	T2
k_{ILD} [N/m]	27.2 ± 0.5	31.4 ± 0.2
c_{ILD} [Ns/m]	2.03 ± 0.32	0.91 ± 0.12
θ_{Mi} [deg]	1.4 ± 0.1	5.0 ± 0.1
$mean(Res)$	0.17×10^{-3}	0.85×10^{-3}
$max(Res)$	45.47×10^{-3}	53.06×10^{-3}
SSR	0.05	1.09
Parameters	T3	T4
k_{ILD} [N/m]	21.2 ± 1.5	21.8 ± 1.8
c_{ILD} [Ns/m]	5.00 ± 1.03	5.00 ± 1.10
θ_{Mi} [deg]	6.4 ± 0.3	4.3 ± 0.4
$mean(Res)$	8.75×10^{-3}	10.16×10^{-3}
$max(Res)$	120.45×10^{-3}	129.70×10^{-3}
SSR	116.65	159.27
Parameters	T5	T6
k_{ILD} [N/m]	28.7 ± 0.4	22.5 ± 0.7
c_{ILD} [Ns/m]	1.58 ± 0.29	4.94 ± 0.46
θ_{Mi} [deg]	7.6 ± 0.1	2.0 ± 0.1
$mean(Res)$	4.35×10^{-3}	3.36×10^{-3}
$max(Res)$	77.85×10^{-3}	65.07×10^{-3}
SSR	28.20	17.70

From the data obtained in Table 6 it is noticeable that the elastic constant varies from 21 [N/m] to 31 [N/m] and the damping coefficient varies from 1.5 [Ns/m] to almost 5 [Ns/m]. Regarding the damping coefficient, its low value does not necessarily imply low dissipation. In fact, for the optimization model, the damping coefficient is responsible only for describing the elongation of the ILD, but after that, all the elastic energy is dissipated due to internal friction, as already shown in Eq. (10).

Interestingly, an inverse relationship is observed between stiffness and damping coefficient: as the stiffness increases, the damping coefficient decreases, and vice versa. This phenomenon can be attributed to the two mechanisms by which elastic energy is dissipated: the first is through the damping coefficient and the second is through the internal friction, as mentioned above. When the elastic coefficient is high, a larger portion of the elastic energy dissipates through internal friction, resulting in a reduced damping coefficient. Conversely, a decrease in the elastic coefficient leads to a higher damping. Thus, the optimization process converges towards two distinct solutions, each offering a valid physical interpretation.

It is also noteworthy to compare the variation of the mean of the residuals for the ILD test and for the initial condition test: they follow the same pattern. This means that the determination of the initial condition has a relevant influence on the final determination of the tuned parameters of the ILD.

The figures presented in this paper depict the experimental data (shown in green) compared to the results of the optimization process (shown in red). The selected comparisons include the barycenter distance, module orientation, and midpoint distance, since these parameters were used in the optimization. Specifically, comparing Fig. 19 and Fig. 16, it can be noticed that in both cases, even at the highest mean value of the residuals, the model effectively estimates the distance to the barycenter.

However, a comparison between Figs. 17 and 20 reveals that this is not entirely true for the orientation of the module. The reason of this discrepancy is mainly due to the fact that during the initial condition optimization process the module is assumed to be static. Nevertheless, by having a close look at Fig. 17 at the beginning the slope of the green curve is different from zero, meaning that there is an initial angular velocity that was not considered in the optimization process.

Finally, in Fig. 21 it can be seen how the model can detect the oscillation of the middle point, particularly the initial peak. In contrast, Fig. 18 does not show this correspondence. This difference is attributed to the higher estimated stiffness coefficient and the lower damping coefficient in T1 compared to the T4 results.

7. Conclusions

This paper provides a short description of the In-Line Damper (ILD) and underscores the significance of characterizing its mechanical response within the context of the E.T.PACK-F project.

The initial part defines a mathematical model that describes the motion of a 3D rigid body connected a system of cables, where at the end the ILD is attached. Subsequently, an experimental setup was implemented at the SPARTANS facility of the University of Padova, where it was possible to emulate the 2D motion of the module, thanks to a 3 m × 2 m testing table and a system of floating platform that almost cancel out the effects of friction. A motion capture system provided the position and orientation of the TM, and from those data it was possible to reconstruct the behavior of the ILD. A simplified 2D mathematical model was then employed to optimize system parameters such as thrust, cable stiffness, and module initial condition.

The results show that the 2D model describes with enough accuracy the ILD elongation, emphasizing the strong non-linearity of the mechanism and its response dependence on the stretch velocity. Finally, the parameters of the stiffness and the damping coefficient of the ILD were retrieved within the limitations posed by the non-linear effects.

CRediT authorship contribution statement

Giulio Polato: Writing – review & editing, Writing – original draft, Software, Investigation, Data curation, Conceptualization. **Matteo Urbinati:** Writing – original draft, Software, Investigation, Conceptualization. **Andrea Valmorbida:** Writing – original draft, Conceptualization, Supervision, Methodology, Formal analysis, Data curation. **Giovanni Anese:** Investigation. **Alice Brunello:** Investigation, Conceptualization. **Samantha Salmistraro:** Investigation. **Sebastiano Chiodini:** Investigation, Formal analysis. **Giacomo Colombatti:** Supervision. **Enrico C. Lorenzini:** Writing – original draft, Supervision.

Declaration of competing interest

The authors declare that they have no known competing financial interests or personal relationships that could have appeared to influence the work reported in this paper.

Acknowledgments

This article was produced while attending the PhD program in PhD in Space Science and Technology at the University of Trento, Cycle XXXIX, with the support of a scholarship financed by the Ministerial Decree no. 118 of 2nd march 2023, based on the NRRP - funded by the European Union - NextGenerationEU - Mission 4 “Education and Research”, Component 1 “Enhancement of the offer of educational services: from nurseries to universities” - Investment 4.1 “Extension of the number of research doctorates and innovative doctorates for public administration and cultural heritage” - CUP E66E23000110001

This work was supported by Horizon Europe EIC Transition Programme under Grant Agreement No. 101058166 (E.T.PACK-F).

References

[1] http://www.etpack.eu (2022).
[2] L. Olivieri, E.C. Lorenzini, A. Valmorbida, A. Brunello, G. Sarego, International extension of patent (PCT), "damper device and connecting apparatus", application number PCT/IB2022/060199. Priority date 25/10/2021, 2021.

[3] A. Valmorbida, M. Mazzucato, S. Tronco, S. Debei, E.C. Lorenzini, SPARTANS-A cooperating spacecraft testbed for autonomous proximity operations experiments, in: 2015 IEEE International Instrumentation and Measurement Technology Conference (I2MTC) Proceedings, IEEE, 2015, pp. 739–744.
[4] S. García González, Avionic System of a Deorbit Kit Based on Electrodynamic Tethers (Ph.D. thesis), Universidad Carlos III de Madrid, 2023.
[5] L. Olivieri, A. Brunello, G. Sarego, A. Valmorbida, E. Lorenzini, An in-line damper for tethers-in-space oscillations dissipation, Acta Astronaut. 189 (2021) 559–566.
[6] A. Valmorbida, M. Mazzucato, S. Tronco, M. Pertile, E. Lorenzini, Design of a ground-based facility to reproduce satellite relative motions, in: 2017 IEEE International Workshop on Metrology for AeroSpace (MetroAeroSpace), IEEE, 2017, pp. 468–473.
[7] A. Valmorbida, M. Mazzucato, M. Pertile, Calibration procedures of a vision-based system for relative motion estimation between satellites flying in proximity, Measurement 151 (2020) 107161.
[8] A. Valmorbida, F. Scarpa, M. Mazzucato, S. Tronco, S. Debei, E.C. Lorenzini, Attitude module characterization of the satellite formation flight testbed, in: 2014 IEEE Metrology for Aerospace (MetroAeroSpace), IEEE, 2014, pp. 73–78.
[9] M. Wang, X. Zhang, W. Tang, J. Wang, A structure for accurately determining the mass and center of gravity of rigid bodies, Appl. Sci. 9 (12) (2019) 2532.